*Journal of the European Ceramic Society* **19** (1999) 2325–2335

PII: S0955-2219(99)00097-7
0955-2219/99/$ - see front matter

# Kinetics of Phase Transformations in SiAlON Ceramics: I. Effects of Cation Size, Composition and Temperature

Anatoly Rosenflanz† and I.-Wei Chen*

Department of Materials Science and Engineering, University of Pennsylvania, Philadelphia, PA 19104-6272, USA

***Abstract***

*Kinetics of direct α/β-$Si_3N_4$→α-SiAlON transformations, reverse α′-SiAlON→β′-SiAlON transformation, and the formation of intermediate phases were investigated for SiAlON ceramics with rare earth stabilizing cations. It was determined that smaller cations (Yb), and α-$Si_3N_4$ starting powders lead to faster $Si_3N_4$→α′-SiAlON transformations. Using the knowledge of phase stability of α′-SiAlON, these observations have been correlated to the overall driving force for the transformation, and the correlation is further extended to the reverse α′-SiAlON→β′-SiAlON transformation. Formation of intermediate phases during $Si_3N_4$→α′-SiAlON transformation is shown to depend on the α′-SiAlON formation and to be inversely correlated to the stability of α′-SiAlON. A thermodynamic interpretation thus emerges to account for the kinetics of SiAlON transformation that encompass the effects of the size of the stabilizing cations, type of starting powder, overall composition, and the reaction temperature.*


*Keywords*: sialon, $Si_3N_4$, phase transformations, kinetics.

## 1 Introduction

Silicon nitride and its derivative SiAlON (solid solutions containing Al and O in addition to Si and N) ceramics constitute an important class of structural ceramics. They are suitable for many commercial applications requiring heat resistance, chemical stability, high toughness and wear durability. Densification of pure silicon nitride is extremely difficult due to the covalent nature of bonding between Si and N. Thus, successful sintering is only possible by applying high pressure, as in hot pressing,[1] or by adding a mixture of oxides (typically $Al_2O_3$ and $Y_2O_3$) which, when heated, react to form a liquid with the silicon dioxide that is invariably present on the surface of each silicon nitride particle.[2]

Densification is usually greatly facilitated by the liquid phase due to enhanced particle rearrangement and the solution-reprecipitation of particles. Liquid-forming oxides can also enter the silicon nitride structure by forming solid solutions commonly referred to as β′-SiAlON and α′-SiAlON. β′-SiAlON solid solution is a substitutional form of β-$Si_3N_4$ structure, with the Al−O bond replacing the Si−N bond, and the basic structure is characterized by the ABAB stacking sequence.[3,4] α′-SiAlON solid solution is produced by replacing some of the Si−N bonds with Al−N and Al−O bonds in the α-$Si_3N_4$ structure, while preserving the ABCDABCD stacking sequence.[5] (Electrical neutrality in the latter solid solution is maintained by adding cations to the interstitial space.) Since formation of both α′-SiAlON and β′-SiAlON requires breaking the Si−N bonds in the starting powders, it, like densification, generally occurs through a solution-reprecipitation mechanism in the presence of the liquid.[6] In this light, the diffusion of atoms in the liquid, the viscosity of the liquid and the solubility of various species in the liquid are important considerations in the kinetics of densification and transformation, as evidenced by the large body of literature on silicon nitride that is devoted to these subjects.[7–9]

Microstructure development in silicon nitride is closely related to the type and kinetics of phase transformation. For instance, when a starting powder with a high α-$Si_3N_4$ phase content is used to produce β-$Si_3N_4$/β′-SiAlON ceramic, the microstructure obtained is characterized by a large proportion of elongated grains;[10] however, an equiaxed microstructure is usually obtained when α-$Si_3N_4$ is used to produce an α′-SiAlON ceramic.[11] This aspect is especially important as it forms the basis for obtaining the high-toughness

*To whom correspondence should be addressed.
†Currently with 3M Corp., St Paul, MN, USA.

$\beta$-$Si_3N_4$/$\beta$-SiAlON that have been in commercial use for some time. Recently, we have also reported the development of an *in-situ* toughened $\alpha'$-SiAlON ceramic.[12] In this case, in contrast to $\beta$-$Si_3N_4$/$\beta'$-SiAlON, the microstructure of elongated $\alpha'$-SiAlON grains can be more readily obtained by using starting powder with a high proportion of $\beta$-$Si_3N_4$ phase,[12] whereas using $\alpha$-$Si_3N_4$ would tend to lead to equiaxed microstructure. Since the composition of $\alpha'$-SiAlON is considerably more complicated and broader than $\beta$-$Si_3N_4$ or $\beta'$-SiAlON, understanding the kinetics of $\alpha/\beta$-$Si_3N_4 \rightarrow \alpha'$-SiAlON transformations is of special interest at this time as it would provide a basis for tailoring the mechanical properties of $\alpha'$-SiAlON through microstructure design.

We have recently presented our general view on the reactions typically occurring in the silicon nitride-SiAlON system.[13] We believe that the most important factor in determining the kinetics of phase evolutions is the magnitude of the thermodynamic driving force, $\Delta G$, for the transformation, as it dictates the rate of nucleation and growth in the kinetics. In this paper, we present a systematic assessment of the way different rare-earth cations (from Nd to Yb) influence the $\alpha/\beta$-$Si_3N_4 \rightarrow \alpha'$-SiAlON transformation kinetics to support the above thesis. Using the same rare-earth cations, we have also studied the effect of the ′-SiAlON composition on the kinetics itself and the reverse transformation of the $\alpha'$-SiAlON$\rightarrow\beta'$-SiAlON type. In the companion paper,[14] we have also undertaken a parallel study of different reaction pathways leading to the same final phase assemblages to provide further support to our kinetic argument. The thermodynamic information referred to in this work is drawn from the phase diagram study reported in a previous paper, which shows the single phase region of $\alpha'$-SiAlON expands as the size of the rare-earth cation decreases and as the temperature increases.

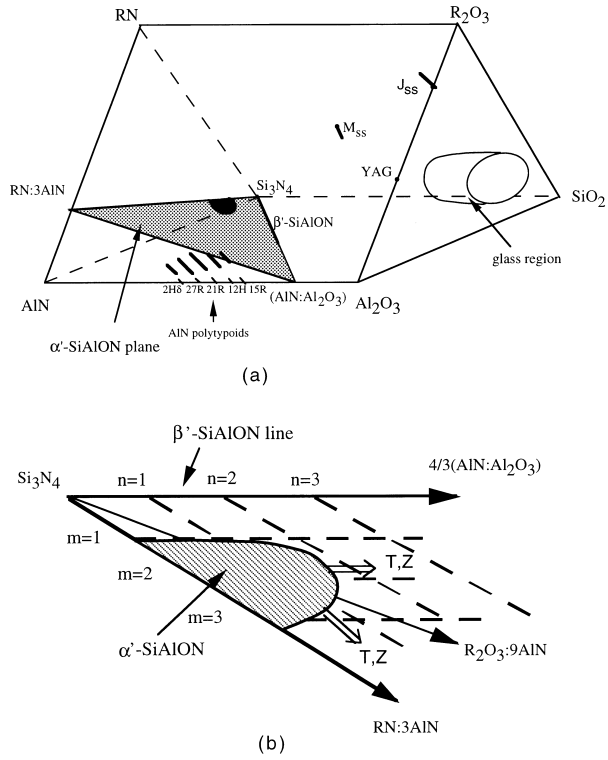


**Fig. 1.** (a) Janecke prism with $\alpha'$-plane highlighted; (b) $\alpha'$-plane with $\alpha'$-SiAlON single phase stability region highlighted.

## 2 Experimental

### 2.1 Composition

The overall compositions studied in this work lie on the so-called $\alpha'$-SiAlON plane, generally defined by the formula $R_{m/3}Si_{12-(m+n)}Al_{m+n}O_nN_{16-n}$. Here, R is a rare-earth cation from the following list: Nd, Sm, Gd, Dy, Y, Er and Yb, in the order of decreasing size. Fig. 1 shows the location of this plane in the Janecke prism together with the $\alpha'$-SiAlON single phase region located on this plane. This single phase region is believed to extend from an interval on the $Si_3N_4$–RN:3AlN line toward the $Si_3N_4$–AlN:$Al_2O_3$ line and the composition therein can be specified in terms of m (corresponding to the rare-earth amount or the number of Al–N bonds) and *n* (corresponding to the oxygen amount or the number of Al–O bonds). As shown in our previous work, the size of $\alpha'$-SiAlON region depends upon the modifying cation and is the smallest for large rare-earths like Nd and Sm and largest for small rare-earths like Yb and Er.[14] It is also temperature dependent and is smaller at lower temperatures.[14]

Most of the materials in the work reported here have a fixed composition $R_{0.4}Si_{9.6}Al_{2.4}O_{1.2}N_{14.8}$, ($m = n = 1.2$) in order to compare the effect of rare-earth ions. This composition will later be referred to as R-1212. In Yb–SiAlON system, we have further studied four different compositions-$(m, n) = (1.2, 1.2)$, $(1.2, 1.8)$, $(0.9, 1.8)$ and $(0.9, 1.2)$—to clarify the effect of composition on phase evolution. These compositions will be referred to as Yb-1212, Yb-1218, etc.

### 2.2 Material

*2.2.1 Powder processing*

Initial powders were fine $\alpha$-$Si_3N_4$ (UBE, SN-E-10), coarse $\alpha$-$Si_3N_4$ (UBE, SN-E-03), fine $\beta$-$Si_3N_4$ (Denki Kagaku, SN-P21FC), $Al_2O_3$ (Sumitomo Chemical America, AKP50), AlN (Tokuyama Soda, Type F), and the various rare-earth oxides $R_2O_3$ (Aldrich Chemical). Table 1 shows the characteristics of the starting silicon nitride powders. The particle size of the fine $\alpha$-$Si_3N_4$ (SN-E-10) powder is essentially identical to that of fine $\beta$-

**Table 1.** Characteristics of silicon nitride starting powders[a]

| *Powder* | *α content (%)* | *Particle size (μm)* | | | *Oxygen content (wt%)* | *Specific surface area ($m^2\ g^{-1}$)* |
|---|---|---|---|---|---|---|
| | | *50%* | *70%* | *90%* | | |
| $\beta$-$Si_3N_4$ (SN-P21FC) | 6·7 | 0·51 | 0·65 | 1·11 | 0·68 | 10·9 |
| $\alpha$-$Si_3N_4$ (SN-E-10) | 95 | 0·5 | 0·7 | 1·33 | 1·5 | 9·4 |
| $\alpha$-$Si_3N_4$ (SN-E-03) | >95 | 1·25 | 1·65 | 2·7 | 0·76 | 3·1 |

[a]Data supplied by manufacturers.

$Si_3N_4$ (Denki Kagaku, SN-P21FC) powder, while particles in $\alpha$-$Si_3N_4$ (UBE, SN-E-03) powder are significantly coarser. These powders were mixed in appropriate amounts to achieve the desired composition, after taking into account the residual oxygen content of $Si_3N_4$ and AlN (data supplied by manufacturers). The powder mixture, in 15 g batches, was attrition-milled in isopropyl alcohol for 2 h using high-purity $Si_3N_4$ milling media in a teflon-coated jar. The slurry was subsequently dried under a lamp while being stirred.

*2.2.2 Hot pressing*

Charges of 3–6 g each were initially cold pressed at 20 MPa into green-body compacts before hot pressing. Hot pressing was performed in a nitrogen atmosphere in a graphite or tungsten resistance furnace. The initial heating rate was 25°C $min^{-1}$ up to 1000°C, followed by a slower rate of 15 °C/$min^{-1}$ to the desired temperature. After the completion of densification, the furnace was shut down to allow rapid cooling. A typical cooling rate was 100°C $min^{-1}$ in the graphite furnace or 350°C $min^{-1}$ in the tungsten furnace. In the above procedure, load was applied when the temperature first reached 1000°C and was kept constant at 30 MPa during the densification stage. During cooling, load was released at 1000°C.

## 2.3 Heat treatment

Kinetics of phase evolutions were studied by reheating previously hot-pressed samples at a rate of 25°C $min^{-1}$ to 1000°C and 15°C $min^{-1}$ to the desired temperature, and then isothermally holding them at that temperature for 45 min. After annealing, the furnace was immediately shut down to allow rapid cooling to room temperature. To minimize the amount of phase transformation occurring during cooling, all annealing experiments were performed in a tungsten resistance furnace, which has a faster cooling rate. Some long annealing experiments at 1500 and 1600°C lasting up to 240 h were also performed in the same furnace.

## 2.4 Phase characterization

X-ray diffraction (XRD) using Cu-$K_\alpha$ radiation, scanning electron microscopy (SEM) and light microscopy were employed for phase identification and microstructural characterization. To estimate the amounts of various phases, the procedure for quantitative XRD analysis as described in Ref. 15 was followed. To avoid the effect of texture on XRD patterns, this analysis was conducted using pulverized powders.

# 3 Results

## 3.1 Fine $\beta$-$Si_3N_4$ powder

We first report the results of phase fractions using $\beta$-$Si_3N_4$ as the starting powder for $Si_3N_4$. There has been very little information in the literature on the kinetics of $\alpha'$ formation starting with $\beta$-$Si_3N_4$ powders (most work reported used $\alpha$ powders). Such information is crucial for the development of *in-situ* toughened $\alpha'$-SiAlON as has been illustrated elsewhere.[12] The samples were hot pressed at 1475°C for 0·5 h and then a set of identical specimens were individually annealed at a higher temperature for 45 min. As shown in Fig. 2, the amount of the dissolved $\beta$-$Si_3N_4$ powder at any given temperature is directly correlated to the

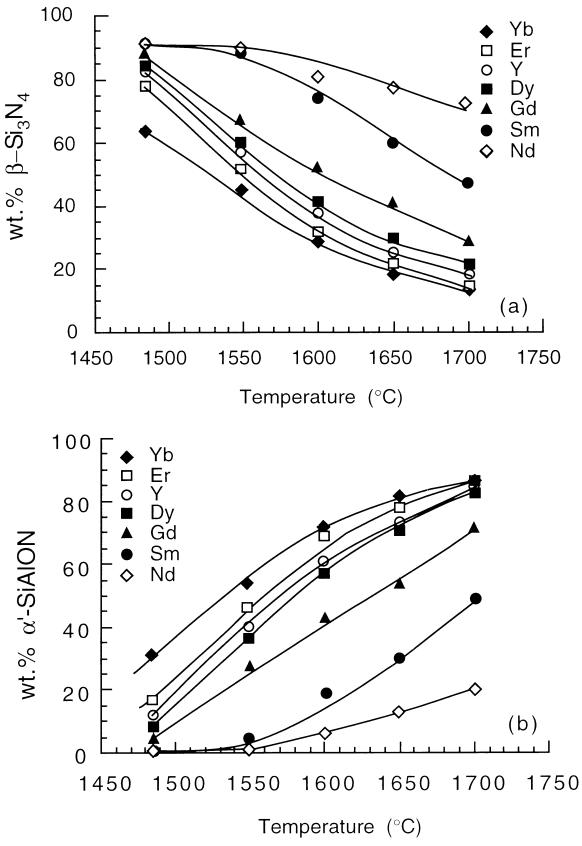


**Fig. 2.** (a) Dissolution of $\beta$-$Si_3N_4$ starting powder; (b) formation of $\alpha'$-SiAlON. Both are shown as functions of temperature. Direct correlation is evident.

amount of the newly formed $\alpha'$-SiAlON. The dissolution of the starting $\beta$-$Si_3N_4$ powder and the formation of $\alpha'$-SiAlON are the fastest for Yb cation (heavier) and the slowest for Nd cation (lighter), as indicated by the higher reaction temperature for the lighter rare-earth cation. This sequence is in the reverse order of the ionic size of cations: Nd > Sm > Gd > Dy > Y > Er > Yb. It should be noted that the above observation is not a result of liquid viscosity, since, for alumina-silicates containing rare earth cations, the viscosity increases with decreasing ionic size.[16] This was verified in our study by the measurement of hot-pressing viscosity and deformation viscosity (see Appendix).

Besides the dissolution of $\beta$-$Si_3N_4$ powder and precipitation of $\alpha'$-SiAlON, formation of intermediate phases was noticed at intermediate temperatures in every rare-earth cation system. The amount and the type of the intermediate phases are shown in Fig. 3. Use of Yb and Er resulted in the formation of garnet ($R_3Al_5O_{12}$) and aluminum nitride polytypoid—12H, while mellilite ($R_2O_3$–$Si_3N_4$ and its solid solution) together with some undissolved AlN was generally observed in compositions containing Gd, Dy, Y, Sm and Nd. These observations are in accord with the reports of Menon and Chen.[17] As noted by these investigators, there are systematic differences in acidity, basicity and wetting behavior of liquid in compositions containing Yb and Er on the one hand (AlN is wetted first by the liquid), and those containing Gd, Dy, Y, Sm and Nd on the other hand ($Si_3N_4$ is wetted first by the liquid), and that these chemical differences cause the formation of different intermediate phases. This seems to be consistent with our observations: garnet, rich in Al, forms with heavier rare-earth cations, while mellilite, rich in Si, forms with lighter rare-earth cations. Also in accordance with the observations of earlier work[18–20] we found that the amount of intermediate phases increased when lighter rare-earth cations were used, reaching about 10 wt% in the case of Nd. However, the amount of the intermediate phases decreases with temperature in all compositions. The rate of this decrease with temperature is faster when heavier modifying cations are used, and the sequence exactly follows that of ionic sizes. The two limiting cases are Yb, where no Yb garnet was found above 1600°C, and Nd, where a significant amount of Nd mellilite was found throughout the temperature range studied (1475 to 1700°C).

Isothermal kinetics were studied at low temperatures using samples previously hot pressed at 1475°C for 0·5 h followed by annealing at 1500°C for up to 240 h or at 1600°C for up to 120 h. These results are shown in Fig. 4. At 1500°C, there is no transformation in Gd, Sm, and Nd materials even after 240 h. For heavier elements, $\beta$-$Si_3N_4$ to $\alpha'$-SiAlON transformation was detected and its amount increased with decreasing ionic radius of the ions. Although the transformation rate appears to decrease with time, the constant slope in the log (time) plot of all the transformation curves indicates that thermodynamic equilibrium had not been achieved at the end of 240 h annealing at 1500°C. This is in contrast to the results shown in Fig. 5 for the transformation at 1600°C, in which the amount of precipitating $\alpha'$-SiAlON appears to have leveled off at a certain value in the case of Yb, Y, Dy and Gd. [The initial slope in log (time) scale exceeds the slope observed at long time, thus indicating saturation.] This end value decreases with increasing ionic size of the rare-earth cations. Given the long annealing time and the apparent saturation of the transformation curves at 1600°C, we believe that equilibrium has been reached at this temperature at the end of annealing. The increasing amount of $\alpha'$-SiAlON with decreasing ionic radii is thus indicative of the higher stability of the $\alpha'$-SiAlON that contains smaller rare-earth ions.

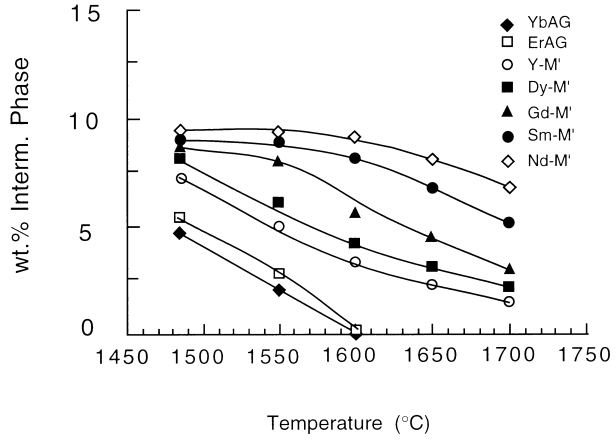


**Fig. 3.** Evolution of intermediate phases during $\beta$-$Si_3N_4 \rightarrow \alpha'$-SiAlON transformation, showing the reluctance of Nd-M′ to dissolve even at higher temperatures.

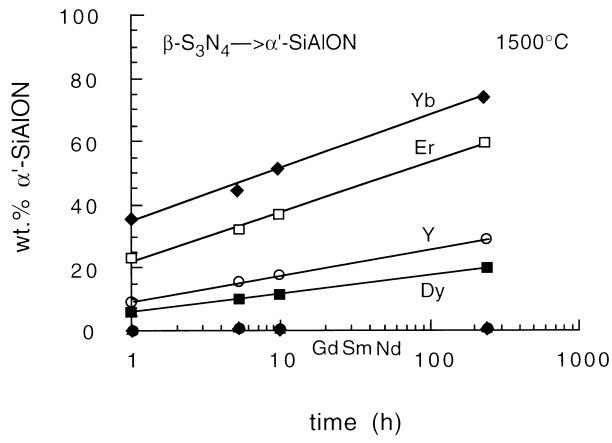


**Fig. 4.** $\alpha'$-SiAlON formation from $\beta$-$Si_3N_4$ powder during isothermal annealing at 1500°C. Transformation does not occur when using Gd, Sm and Nd as stabilizing cations.

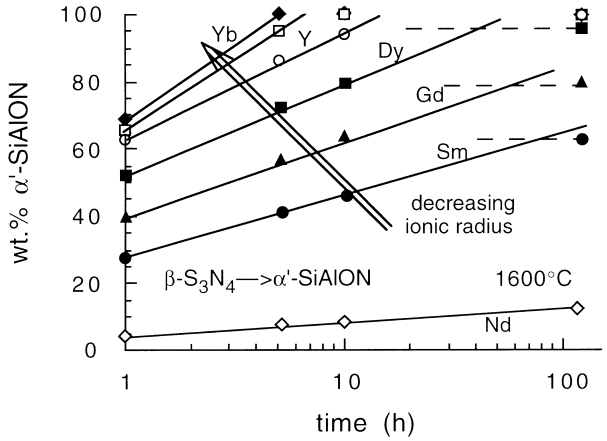


**Fig. 5.** $\alpha'$-SiAlON formation from $\beta$-$Si_3N_4$ powder during isothermal annealing at 1600°C. The dotted line indicates the apparent saturated amount, as supported by the data of $\alpha \rightarrow \alpha'$ transformation (see Fig. 8).

### 3.2 Fine $\alpha$-$Si_3N_4$ powder (UBE, SN-E-10)

The results of transformation kinetics using fine $\alpha$-$Si_3N_4$ as starting powders (UBE E-10) are summarized in Fig. 6. These samples were previously hot pressed at 1475°C for 0·5 h and then annealed at a higher temperature for 45 min. The general trend regarding $\alpha$-$Si_3N_4$ dissolution, $\alpha'$ formation, formation of intermediate phase and variation with rare earth cations is similar to those seen in experiments with $\beta$-$Si_3N_4$ as starting powders (refer to Figs 2 and 3). Namely, $\alpha$ dissolution is directly correlated to $\alpha'$ formation, the $\alpha \rightarrow \alpha'$-SiAlON reaction occurs at lower temperatures for smaller rare earth ions, the amount of intermediate phase is less for smaller rare earth cations and at higher temperatures, and the intermediate phase changes from mellilite to garnet as the rare-earth ions decrease in size. On the other hand, a comparison between Figs 6 and 2 indicates that the formation of $\alpha'$-SiAlON from $\alpha$-$Si_3N_4$ starting powder generally proceeds at a lower temperature than when the starting powder is $\beta$-$Si_3N_4$. For instance, when the starting powder is $\alpha$-$Si_3N_4$, the formation of $\alpha'$-SiAlON is complete at 1600°C for all compositions except Gd, Sm and Nd. This compares with the highest amount of $\alpha'$-SiAlON of 72%, achieved in the Yb system, when $\beta$-$Si_3N_4$ powder was used at the same temperature. This difference is not caused by the size of the powders, which is frequently quoted in the literature on $Si_3N_4$.[21] The average particle size of $Si_3N_4$ (about 0·5 $\mu$m, see Table 1) is essentially the same in the two starting powders in these experiments.

The kinetic advantage of using $\alpha$-$Si_3N_4$ powder was also demonstrated in isothermal annealing experiments at either 1500°C for up to 240 h or 1600°C for up to 120 h. As seen from Fig. 7, the $\alpha \rightarrow \alpha'$-SiAlON transformation occurs quite readily at 1500°C in all rare-earth systems except Nd.

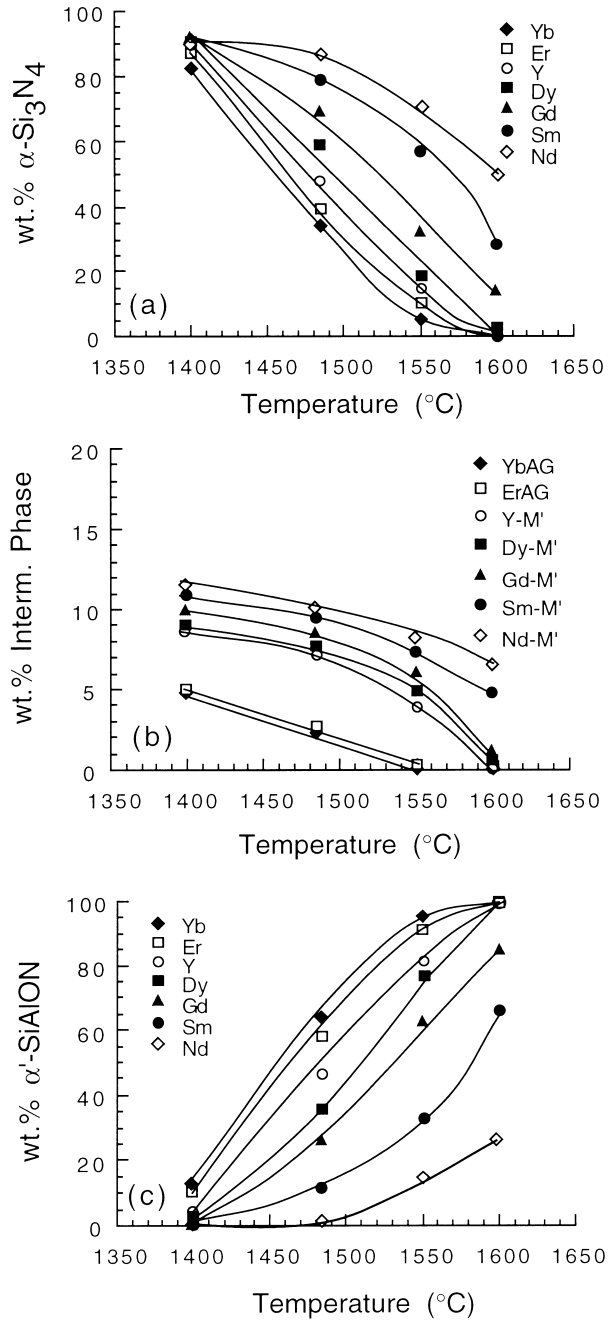


**Fig. 6.** (a) Dissolution of $\alpha$-$Si_3N_4$ (E10) powder; (b) evolution of intermediate phases; and (c) formation of $\alpha'$-SiAlON; as functions of temperature.

Indeed, the reaction appears to level off in at least Yb, Er, Y, Dy and probably Gd–SiAlON systems, in contrast to the continuing reactions seen in Fig. 4. It should be noted that, in all cases, at the end of 240 h annealing at 1500°C, the balance phase is $\beta'$-SiAlON. No $\alpha$-$Si_3N_4$ starting powder remains at this point. Figure 8 further demonstrates the faster kinetics of $\alpha$-$Si_3N_4 \rightarrow \alpha'$-SiAlON transformation. After holding at 1600°C for 1 h, $\alpha \rightarrow \alpha'$ transformation is essentially complete for all modifying rare-earth cations except Nd, which is completed in less than 10 h. Importantly, we found that the saturation levels of $\alpha'$-SiAlON at 1600°C in Fig. 8 are the same as those in Fig. 5 for all the rare earth

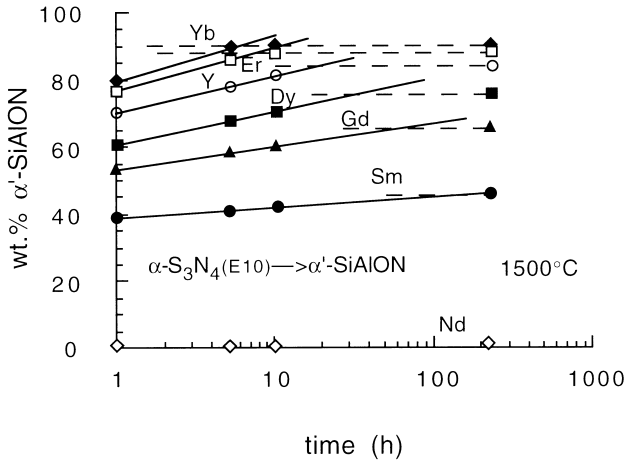


**Fig. 7.** $\alpha'$-SiAlON formation from $\alpha$-$Si_3N_4$ powder (E10) during isothermal annealing at 1500°C.

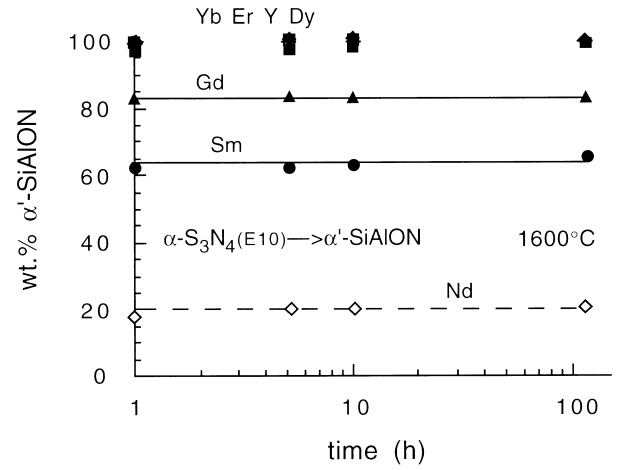


**Fig. 8.** $\alpha'$-SiAlON formation from $\alpha$-$Si_3N_4$ powder (E10) during isothermal annealing at 1600°C. Note the similar amounts of $\alpha'$-SiAlON formed at 1600°C from α-powder (given by this figure) and $\beta$-powder (given by Fig. 5), indicating thermodynamic equilibrium.

ions, even though the starting $Si_3N_4$ powders are different. (Nd-SiAlON did not reach saturation in Fig. 5.) This strongly suggests that equilibrium has been reached at 1600°C after 120 h in the cases of Yb, Er, Y, Dy, Gd, and Sm regardless of the starting $Si_3N_4$ powder. The different values of equilibrium $\alpha'$ amount also establish the different stability of $\alpha'$-SiAlON with different rare-earth cations. In addition, comparing Figs 7 and 8, we can see that there is more $\alpha'$-SiAlON at 1600°C than at 1500°C. Thus, the stabiltiy of $\alpha'$-SiAlON increases with temperature.

### 3.3 Coarse $\alpha$-$Si_3N_4$ powder (UBE, SN-E-03)

We have also verified the above results on the transformation kinetics using a coarse $\alpha$-$Si_3N_4$ powder (UBE SN-E-03). The amount of $\alpha'$-SiAlON at a given temperature is, of course, lower when using a coarser powder. This can be seen by comparing Fig. 9 (coarser powder) with Fig. 6 (finer powder). However, the shape and trend of

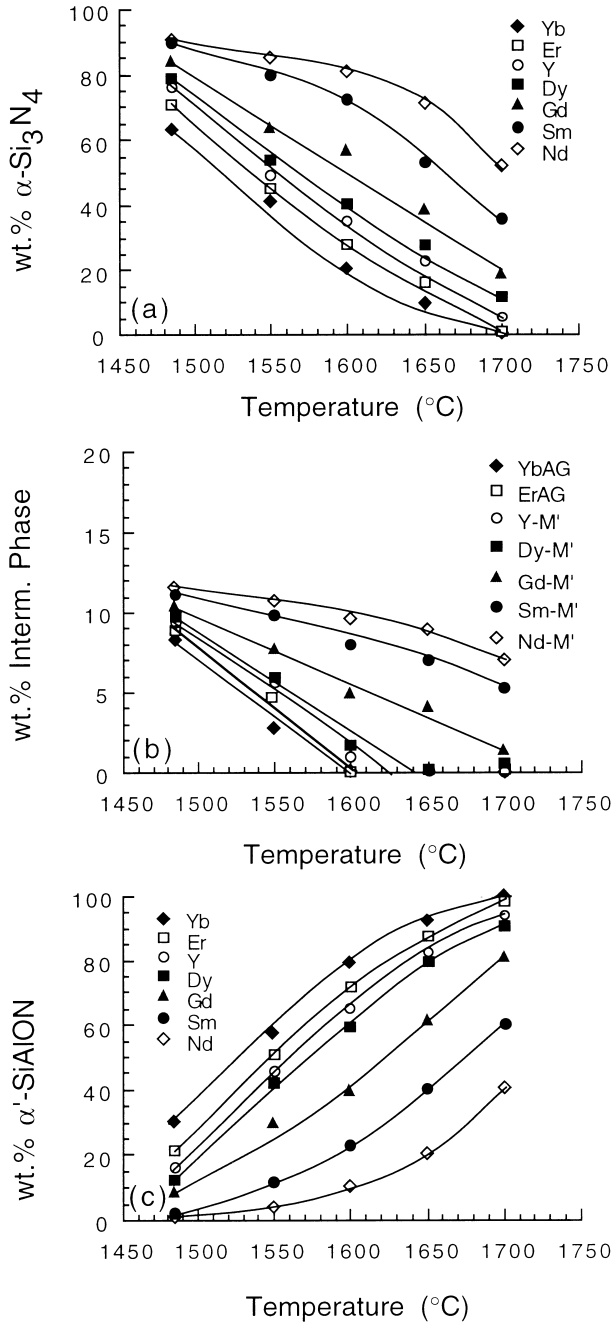


**Fig. 9.** (a) Dissolution of $\alpha$-$Si_3N_4$ (E03) powder; (b) evolution of intermediate phases, and (c) formation of $\alpha'$-SiAlON; as functions of temperature.

the transformation curves in Fig. 9 are very similar to those of Fig. 6. In fact, if all the transformation curves in Fig. 6(c) are shifted by about 100°C, then the kinetics of the coarse and fine powders become quite comparable. A slower rate of dissolution of the coarser $\alpha$-E-03 powder compared to E-10 powder is apparently the cause of the above systematic difference.

### 3.4 Yb-compositions

We further studied the kinetics of $\beta$-$Si_3N_4$→$\alpha'$-SiAlON transformation at several compositions on the $\alpha'$-plane in Yb-containing systems (see inset in Fig. 10). As indicated in Table 2, these materials contained mostly $\alpha'$-SiAlON after annealing at

1950°C for 1·5 h. Only a very small amount of $\beta'$-SiAlON was present in compositions Yb-0918 and Yb-0912. Despite a similar phase assemblage at equilibrium, however, the kinetics of forming $\alpha'$-SiAlON were quite different. As illustrated in Fig. 10, compositions of a fixed n form $\alpha'$-SiAlON at a lower temperature when m is higher, i.e. when a higher amount of $(RAl_3)N_4$ is present. This can be seen by comparing Yb-0912 and Yb-1212, and likewise Yb-0918 and Yb-1218. Also, comparing compositions of a fixed *m* but different *n*, we see that the $\beta$-$Si_3N_4 \rightarrow \alpha'$-SiAlON transformation occurs at a lower temperature when *n* decreases, i.e. when a lower amount of oxygen or Al–O bonds are present. For example, the reaction proceeded to a larger extent for Yb-1212 and Yb-0912 compositions compared to Yb-1218 and Yb-0918. These latter observations are quite surprising because they do not agree with the general perception that the transformation kinetics in $Si_3N_4$/SiAlON system are faster in the presence of a higher amount of liquid phase.[22] (Yb-1218 and Yb-0918 compositions are richer in $Al_2O_3$ than Yb-1212 and Yb-0912, respectively. Nevertheless, the higher amount of $Al_2O_3$ did not facilitate $\alpha'$-SiAlON formation.)

### 3.5 Reverse transformations

Materials of all compositions, previously heat-treated at 1950°C, were subsequently annealed at low temperatures (1600 and 1500°C) for a prolonged period of time (120 and 240 h, respectively). Before the low temperature annealing, all materials contained more than 90 wt% $\alpha'$-SiAlON. Figure 11(a) shows that, during annealing at 1600°C for 120 h, $\alpha'$-SiAlON stabilized with lighter rare-earth cations (Nd and Sm) exhibited reverse transformation of the $\alpha' \rightarrow \beta'$-SiAlON type. However, this reverse transformation did not proceed extensively, accounting only for 20 wt% of the initial $\alpha'$-SiAlON in the Nd case. The small amounts of $\beta'$-SiAlON formed are shown in Fig. 11. It has the composition $Si_{5.6}Al_{0.4}O_{0.4}N_{7.6}$ as determined by X-ray technique. At the same time, $\alpha'$-SiAlON stabilized by heavier rare-earth cations (like Y, Dy, Er and Yb) remained essentially untransformed. During annealing at 1500°C for 240 h, $\alpha' \rightarrow \beta'$-SiAlON reverse transformation proceeded more readily in all materials except those containing Yb and Er, as shown in Fig. 12. Comparing the slope in the semi-log scale in Figs 11 and 12, we also see a faster transformation rate in Fig. 12 despite the lower temperature. Again, the transformation was more extensive in Nd material, and it progressively decreases as the size of the stabilizing cation decreases.

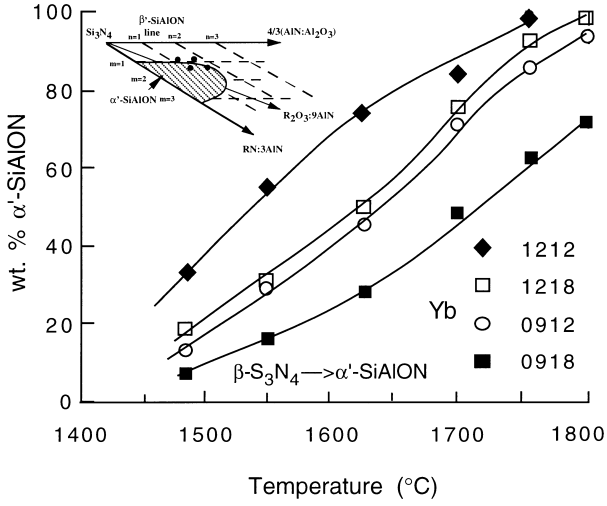


**Fig. 10.** Formation of $\alpha'$-SiAlON in materials with Yb-compositions shown on the inset picture as dots.

**Table 2.** Phase assemblage of Yb-materials prepared at 1950°C

| *Composition* | *α′-SiAlON wt%* | *β′-SiAlON wt%* |
|---|---|---|
| Yb-1212 | 100 | 0 |
| Yb-1218 | 100 | 0 |
| Yb-0912 | 95 | 5 |
| Yb-1918 | 95 | 5 |

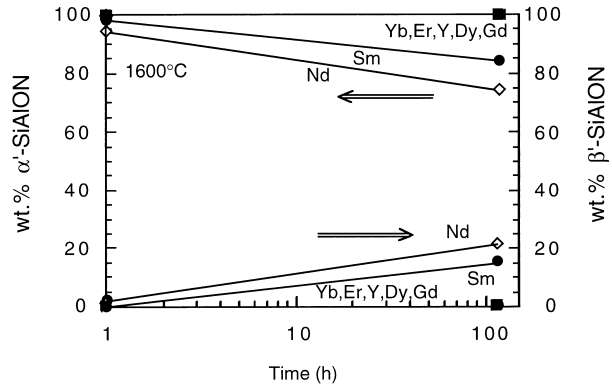


**Fig. 11.** Dissolution of $\alpha'$-SiAlON and formation of $\beta'$-SiAlON during reverse transformation at 1600°C.

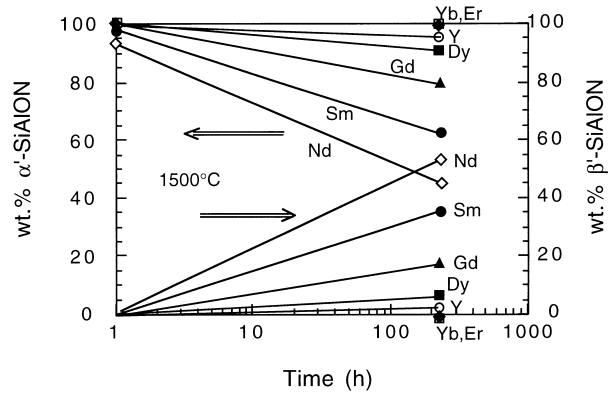


**Fig. 12.** Dissolution of $\alpha'$-SiAlON during reverse transformation at 1500°C. Higher rates compared to that of transformation at 1600°C are evident by comparison with Fig. 11.

## 4 Discussion

### 4.1 Correlation between kinetics and driving force

The results of this study clearly demonstrate that the kinetics of $\alpha/\beta \rightarrow \alpha'$-SiAlON transformation are accelerated when smaller cations are used for stabilizing $\alpha'$-SiAlON phase. This chemical aspect cannot be attributed to the liquid viscosity since silicate liquids containing larger cations (of a lower field strength) typically show a lower viscosity, which would be expected to enhance transformation kinetics.[22] The opposite was observed here. In the following we will examine the thermodynamics of these transformations and show that the faster kinetics is always correlated to more favorable energetics.

We have already reported in a previous paper[14] our finding of a decreased stability of $\alpha'$-SiAlON phase with decreasing temperature and increasing size of rare-earth cation. These results are supported by our long-term annealing experiments at 1500 and 1600°C in this study. Materials with a fixed (1212) composition but different modifying cations contain more $\alpha'$-SiAlON when smaller rare-earth cations are used, and the amount of equilibrated $\alpha'$-SiAlON is higher at higher annealing temperatures. The above results have been incorporated in the phase diagram for Nd, Y and Yb-SiAlON at 1950°C shown in Fig. 13. The larger single phase $\alpha'$ region is reflected not only along the $Si_3N_4$–$R_2O_3$:9AlN line ($m = 1{\cdot}79$ in Nd, 2·6 in Y and 3·0 in Yb cases) but also at the apex ($n = 1{\cdot}1$ in Nd-$\alpha'$-SiAlON, 1·6 in Y-$\alpha'$-SiAlON, and 1·8 in Yb-$\alpha'$-SiAlON). The single phase boundary recedes at lower temperature especially in the case of Nd-SiAlON and especially around the apex.[14] As shown in Fig. 14, there is a direct connection between solubility range and phase stability. This can be established by drawing common tangents between the free energy curves of $\alpha'$-SiAlON and those of neighboring phases. It can then be seen that a larger single phase $\alpha'$ region corresponds to a lower overall free energy of $\alpha'$-SiAlON. Applying this concept to the size effect, we can expect, for example, a lower overall free energy of $\alpha'$-SiAlON phase in the Yb-containing system than in the Nd-containing system. Likewise, applying this concept to the temperature effect, we expect a lower overall free energy of $\alpha'$-SiAlON relative to $\beta$-$Si_3N_4$ as the temperature increases. This lower free energy would then result in a larger driving force, $\Delta G$, for $\alpha/\beta \rightarrow \alpha'$-SiAlON transformation, favoring smaller cations and higher temperatures.

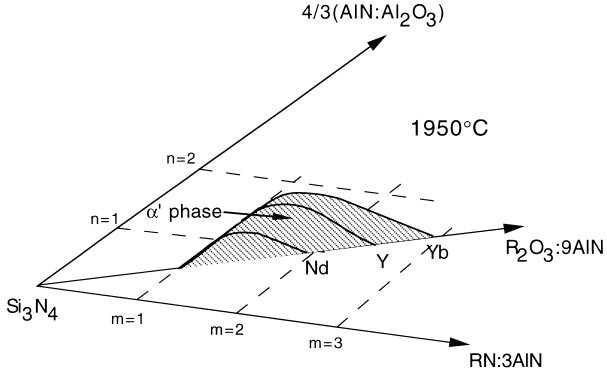


**Fig. 13.** $\alpha'$ phase region in the $Si_3N_4$ corner at 1950°C. Much larger stability region exists for Yb cation than for Nd cation.

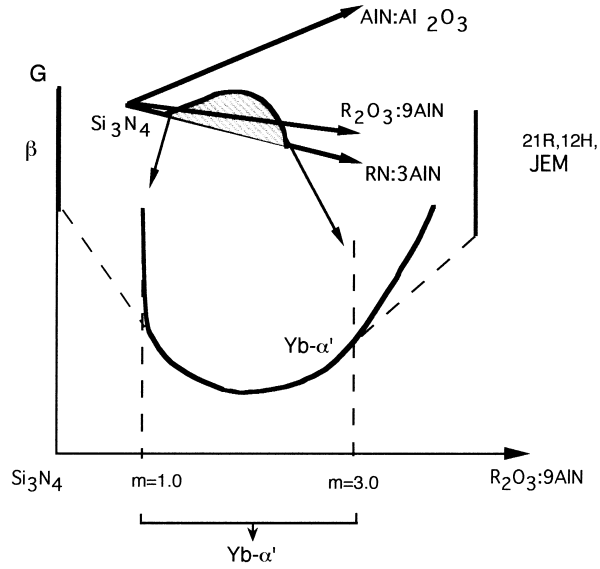


**Fig. 14.** Pseudo-binary free energy diagram indicating decrease higher thermodynamic driving force for $\beta$-$Si_3N_4$→Yb-$\alpha'$-SiAlON transformation. This binary diagram is incomplete in that it only shows $\beta$-$Si_3N_4$, $\alpha'$-SiAlON and a third phase (21R, 12H or JEM). In reality, a third compositional component ($AlN:Al_2O_3$) and another phase (e.g. glass or liquid) which also has a broad range of composition should also be included.

Faster kinetics observed for transformations in materials containing smaller rare earth cations are obviously consistent with the argument of the larger driving force. In the $\alpha/\beta \rightarrow \alpha'$-SiAlON transformation, however, the temperature effect might be regarded as coincidental since a higher temperature also provides more thermal activation. In this context, the faster reverse transformation at lower temperatures offers an unambiquous example of the direct correlation between driving force and kinetics. Since $\Delta G$ for $\alpha'$-SiAlON→$\beta/\beta'$ SiAlON is essentially the opposite of that for $\alpha/\beta \rightarrow \alpha'$-SiAlON transformation, it increases with increasing size of rare earth cation and with decreasing temperature. Thus, the faster reverse transformation at lower temperature which has less thermal activation, can be attributed to the higher driving force. The ionic size effect in the reverse transformation, i.e. faster kinetics for the Nd case than for Sm and other cations, is also in direct correlation with the magnitude of the driving force.

Lastly, the argument of driving force also applies to the observations in Fig. 10 involving four compositions of Yb-SiAlON. Referring to Fig. 14, we see that the $\alpha'$-SiAlON of a compostion further in the single phase $\alpha'$ region has a lower free energy than that near the phase boundary. As seen in the inset of Fig. 10, of the four compositions studied, the ones that have a higher m value and a lower n value are located more toward the center of the single phase $\alpha'$-SiAlON region and farther from the phase boundary. Thus, they have higher phase stability, larger $\Delta G$ for $\alpha/\beta \rightarrow \alpha'$-SiAlON transformation, and faster kinetics as observed. As we already mentioned in Section 3.4, the conventional thinking based on oxygen content and liquid amount would have predicted the exact opposite for the kinetics of these four compositions.

The direct correlation between transformation kinetics and transformation driving force can be rationalized using the standard theory of phase transformation. All the reactions considered here, $\alpha/\beta$-$Si_3N_4 \rightarrow \alpha'$-SiAlON and $\alpha'$-SiAlON$\rightarrow\beta/\beta'$-SiAlON, are the first order transitions as evidenced for instance in Figs 4 and 5 where the fraction of a newly formed phase is linearly dependent on ln $t$ (recall Avrami eqn). Therefore, their kinetics involve the stages of nucleation and growth. Both the rate of nucleation and the rate of growth are known to increase with the driving force. In particular, a very strong, non-linear dependence on $\Delta G$ is expected for the nucleation rate. So, the correlation between driving force and faster transformation kinetics is reasonable, and the driving force argument can be used to explain the effect of temperature and compositions (including different cations) in both forward and reverse transformations. Moreover, this argument is consistent with the observation that the kinetics of $\alpha'$-SiAlON formation are accelerated when the starting silicon nitride powder is $\alpha$-$Si_3N^4$. This is because $\alpha$-$Si_3N_4$ is believed to be less stable than $\beta$-$Si_3N_4$,[23] thus a higher driving force for $\alpha'$-SiAlON formation is available when $\alpha$-$Si_3N_4$ is used as the starting powder. Of course, heterogeneous nucleation of $\alpha'$-SiAlON on $\alpha$-$Si_3N_4$ has been observed[24] and it would provide additional kinetic advantages given the structural similarity of $\alpha$-$Si_3N_4$ and $\alpha'$-SiAlON. The latter effect, however, is in the same direction as the driving force effect in the case of $\alpha'$-formation and should not cause any competition and reversal of trends. To further differentiate the effect of $\alpha$- and $\beta$-$Si_3N_4$ starting powders, other transformation paths need to be investigated. Such a study will be reported in the companion paper.

### 4.2 Kinetics of formation of intermediate phases

There have been several related observations in the recent literature regarding the kinetics of $\alpha'$-SiAlON formation and the intermediate phase evolutions.[18–20] There has also been considerable attention paid to the reverse transformation of $\alpha'$-SiAlON.[25,26] All of these studies, to our knowledge, have been performed using $\alpha$-$Si_3N_4$ as starting powders. Since we have already reviewed the kinetics of reverse transformation elsewhere,[14] and described the kinetics of $\alpha'$ formation above,we focus the following discussion on the kinetics of formation of intermediate phases only.

Slasor *et al.*[18] have proposed that the effect of cation size on $\alpha'$-formation may be attributed to the formation of the rare-earth rich phases, like mellilite. These and other authors[19,20] argue that, in lighter rare-earth cation systems, mellilite forms at intermediate temperatures more readily than $\alpha'$-SiAlON, therefore depriving $\alpha'$-SiAlON of the necessary stabilizing cation and delaying the $\alpha \rightarrow \alpha'$-SiAlON transformation. It is our understanding, however, that the preferred formation of intermediate phases in light rare-earths systems is directly related to the decreased stability of the $\alpha'$-SiAlON phase for such cations. Thus, it should be considered as a consequence of the evolution of $\alpha'$-SiAlON phase rather than the cause. For instance, the fact that no Nd-$\alpha'$-SiAlON formation was registered at 1500°C suggests that $\alpha'$-SiAlON either simply does not exist in the phase diagram at this temperature, or it is confined to a very small area close to the $Si_3N_4$–$R_2O_3$:9AlN line or even below the line, and is thus not accessible in most experiments. As a result, formation of mellilite is favored due to the availability of Nd cation in the composition, and it is indeed an equilibrium phase rather than a metastable phase. It is seen in Fig. 3 that

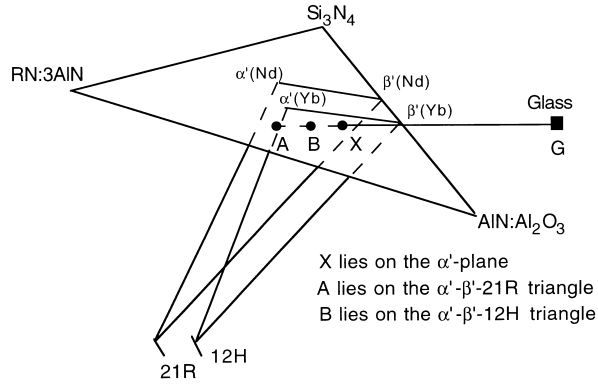


**Fig. 15.** Schematic phase relationships showing the effect of cation and temperature, giving different glass amounts according to the lever rule. At the same temperature, the base triangle ($\alpha'$–$\beta'$-AlN polytype) in the $\alpha'$–$\beta'$-AlN polytype-glass tetrahedron lies closer to the $Si_3N_4$–AlN:3AlN line in the Nd system than in the Yb system. Thus, the point (X) on $\alpha'$-plane has a projection of GX that is further away in the Nd system (A) than in the Yb system (B). In the same system, the base triangle ($\alpha'$–$\beta'$-AlN polytype) in the $\alpha'$–$\beta'$-AlN polytype-glass tetrahedron lies closer to the $Si_3N_4$–AlN:3AlN line at lower temperature than at high temperature.

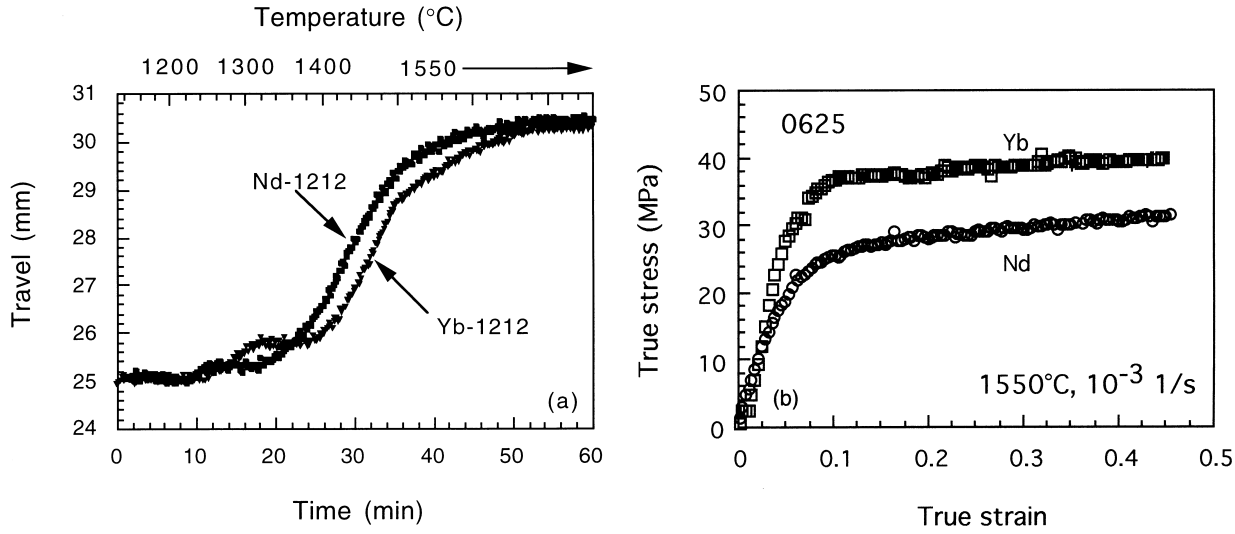


**Fig. 16.** (a) Shrinkage curves for materials with Nd-1212 and Yb-1212 compositions. Faster densification is evident for the former composition, indicating lower viscosity of the glass in Nd system than in Yb system. (b) Flow stress versus true strain in compression for Nd-0625 and Yb-0625 materials at 1550°C. Lower flow stress in the case of Nd indicates lower viscosity of the glass in this system.

mellilite persists in this Nd material until $\alpha'$-SiAlON phase becomes more stable (which happens at around 1700°C), and it totally disappears at higher temperatures when the single phase $\alpha'$-SiAlON region expands sufficiently. This suggests that $\alpha'$-SiAlON first forms in the appropriate amount (largely dictated by the phase diagram at the particular temperature) and the balance rare-earth cations enter mellilite or other intermediate phases. This argument is further supported by the observation that mellilite is more stable in materials with larger modifying cations, like Nd, Gd and Dy, which have smaller single phase regions for the $\alpha'$-SiAlON. (The range of stability of melilite solid solutions at higher temperatures has been outlined elsewhere.[27,28])

The above argument can be made more quantitative by referring to the compatibility tetrahedra ($\alpha'$–$\beta'$-AlN polytypoid-glass) shown in Fig. 15. Here the polytypoid is the 21R type in the Nd case and 12H in the Yb case. As we described in a previous paper,[14], the $\alpha'$–$\beta'$ phase line tend to move toward RN:3AlN line at lower temperatures and for larger cations. As this movement occurs, any point (X in Fig. 15) on the $\alpha'$-plane that lies within the tetrahedron will find its distance to the projection of the GX line in Fig. 15 on the base triangle ($\alpha'$–$\beta'$-AlN polytypoid) to increase. Therefore, according to the lever rule, the fraction of glass (e.g. XA/GA in the Nd case versus XB/GB in the Yb case) increases. Since at lower temperature this glass forms one of the intermediate phases, the amount of such intermediate phase is expected to increase at lower temperature and with larger cations. This result can thus be explained in terms of the phase relations and may not have anything to do with kinetics. The overall kinetics including that of $\alpha'$-SiAlON and intermediate phases appear to be governed by the energetics of $\alpha'$-SiAlON only.

## 5 Conclusions

- $\beta/\alpha \rightarrow \alpha'$-SiAlON transformation proceeds faster with smaller modifying cations which stabilize $\alpha'$-SiAlON more, thus providing a larger driving force for the transformation.
- $\beta$-$Si_3N_4 \rightarrow \alpha'$-SiAlON transformation proceeds slower than $\alpha$-$Si_3N_4 \rightarrow \alpha'$-SiAlON transformation, because $\beta$-$Si_3N_4$ is more stable than $\alpha$-$Si_3N_4$, thus providing a lower driving force.
- Formation of intermediate phases follows that of $\alpha'$-SiAlON, with an amount that is in inverse proportion to the stability of $\alpha'$-SiAlON and hence in direct correlation to the stability of the intermediate phase.
- Kinetics of reverse $\alpha'$-SiAlON$\rightarrow\beta'$-SiAlON transformation is faster for larger modifying cations and at lower temperature, again because a larger driving force (for reverse transformation) is available in these cases.

## Acknowledgements

This work was supported by the Air Force Office for Scientific Research, Grant no. F49620-98-1-0126. The use of facilities in the Laboratory for Research on the Structure of Matter at the University of Pennsylvania, supported by the National Science Foundation under MRSEC Grant no. DMR 96-32598, is also acknowledged.

## References


1. Deeley, G. G., Herbert, J. M. and Moore, N. C., Dense silicon nitride. *Powder Metall.*, 1961, **8**, 145–151.
2. Komeya, K. and Inoue, H., Heat resistant strengthened composites. Japanese patent no. 703695, 1969.
3. Oyama, Y. and Kamigaito, O., Solid solubility of some oxides in $Si_3N_4$. *Jpn. J. Appl. Phys.*, 1971, **10**, 1637–1642.
4. Jack, K. H. and Wilson, W. I., Ceramics based on the Si–Al–O–N and related systems. *Nature: Phys. Sci.*, 1972, **238**, 28–29.
5. Hampshire, S., Park, H. K., Thompson, D. P. and Jack, K. H., $\alpha'$-SiAlON ceramics. *Nature*, 1978, **274**, 880–882.
6. Henderson, C. M. B. and Taylor, D., Thermal expansion of the nitrides and oxynitride of silicon in relation to their structures. *Trans. J. Brit. Ceram. Soc.*, 1975, **74**(2), 49–53.
7. Greskovich, C., Prochazka, S. and Rosolowski, J. H., Basic research on silicon nitride ceramics. General Electric Rept. SRD-76-036, March 1976.
8. Boskovic, S., Gauckler, L. J., Petzow, G. and Tien, T. Y., Reaction sintering forming $\beta$-$Si_3N_4$ solid solutions in the system Si,Al/N,O: sintering of $Si_3N_4$–AlN–$Al_2O_3$ mixture. *Powder Met. Int.*, 1979, **11**(4), 169–170.
9. Rossowsky, R., Wetting of silicon nitride by alkaline-doped $MgSiO_3$. *J. Mater. Sci.*, 1974, **9**(12), 2025–2033.
10. Lange, F. F., Fracture toughness of $Si_3N_4$ as a function of the initial $\alpha$-phase content. *J. Am. Ceram. Soc.*, 1979, **62**(7–8), 428–430.
11. Ekstrom, T. and Nygren, M., SiAlON ceramics. *J. Am. Ceram. Soc.*, 1992, **75**(2), 259–276.
12. Chen, I-W. and Rosenflanz, A., *In-situ* toughened $\alpha'$-SiAlON ceramics. *Nature*, 1997, **389**, 701–704.
13. Rosenflanz, A. and Chen, I.-W., Kinetics of phase transformations in SiAlON ceramics. Presented at the 99th Annual Meeting of the American Ceramic Society 6 May 1997, Cincinnati, OH.
14. Rosenflanz, A. and Chen, I.-W., Phase relationships and stability of $\alpha'$-SiAlON. *J. Am. Ceram. Soc.*, 1999, **82**(4), 1025–1036.
15. Gazzara, C. P. and Messier, D. R., Determination of phase content of $Si_3N_4$ by X-ray diffraction analysis. *J. Am. Ceram. Soc. Bull.*, 1977, **56**(9), 777–780.
16. Shelby, J. E. and Kohli, J., Rare-earth aluminosilicate glasses. *J. Am. Ceram. Soc.*, 1990, **73**(1), 39–42.
17. Menon, M. and Chen, I.-W., Reaction densification of $\alpha'$-SiAlON: I, wetting behavior and acid-base reactions. *J. Am. Ceram. Soc.*, 1995, **78**(3), 545–552.
18. Slasor, S. and Thompson, D. P., Preparation and characterization of yttrium $\alpha'$-SiAlONs. In *Non-oxide Technical and Engineering Ceramics*, ed. S. Hampshire. Elsevier Applied Science, Barking, UK, 1986, pp. 223–230.
19. Hampshire, S., O'Reilly, K. P. J., Leigh, M. and Redington, M., Formation of $\alpha'$-SiAlONs with neodymium and samarium modifying cations. In *High-Tech Ceramics*, ed. P. Vincenzini. Elsevier, Amsterdam, 1987, pp. 933–940.
20. O'Reilly, K. P. J., Redington, M., Hampshire, S. and Leigh, M., Parameters affecting pressureless sintering of $\alpha'$-SiAlONs with lanthanide modifying cations. *Mater. Res. Soc. Symp. Proc.*, 1992, **287**, 393–398.
21. Kato, A., Sarugaku, K. and Sameshima, S., Sinterability of silicon nitride powders. In *High-Tech Ceramics*, ed. P. Vincenzini. Elsevier, Amsterdam, 1987, pp. 911–924.
22. Hwang, S.-L. and Chen, I.-W., Reaction hot-pressing of $\alpha'$-and $\beta'$-SiAlON ceramics. *J. Am. Ceram. Soc.*, 1994, **77**(1), 165–171.
23. Grun, R., The crystal structure of $\beta$-$Si_3N_4$; structural and stability considerations between $\alpha$- and $\beta$-$Si_3N_4$. *Acta Cryst. B*, 1979, **35**, 800–804.
24. Hwang, S.-L. and Chen, I.-W., Nucleation and growth of $\alpha'$-SiAlON on $\alpha$-$Si_3N_4$. *J. Am. Ceram. Soc.*, 1994, **77**(7), 1711–1718.
25. Mandal, H., Thompson, D. P. and Ekstrom, T., Reversible $\alpha \Rightarrow \beta$-SiAlON transformation in heat-treated SiAlON ceramics. *J. Eur. Ceram. Soc.*, 1993, **12**, 421–429.
26. Thompson, D. P., $\alpha \Rightarrow \beta$-SiAlON transformation. In *Tailoring Of Mechanical Properties of $Si_3N_4$ Ceramics*, ed. M. J. Hoffman and G. Petzow. Academic Publishers, The Netherlands, 1994, pp. 125–137.
27. Cheng, Y.-B. and Thompson, D. P., Al-containing nitrogen melilite phases. *J. Am. Ceram. Soc.*, 1994, **77**(1), 143–148.
28. Huang, Z.-K. and Chen, I.-W., Rare earth melilite solid solution and its phase relations with neighboring phases. *J. Am. Ceram. Soc.*, 1996, **79**(8), 2091–2097.


## Appendix

As shown in Fig. 16(a), the densification rates during hot-pressing are affected by the choice of the rare-earth cation and are faster for Nd-1212 composition than for Yb-1212 composition. This is taken as the evidence of a lower viscosity of the liquid phase with Nd than with Yb. In support of this conclusion, we also present here the results of deformation study of Nd-0625 and Yb-0625 materials. The Nd material has a lower flow stress than the Yb material under identical deformation conditions in the compression experiments [see Fig. 16(b)]. The lower viscosity of the melt that contains larger rare-earth cations is presumably due to the lower field strength of the larger cations. This is known to cause lower strength and higher $T_g$ of the glass.[16] In the present study, although a lower viscosity should in principle facilitate phase transformation, we have found many examples that contradicted the above expectation because of the overriding consideration of the thermodynamic stability of the product phase.